https://doi.org/10.5194/egusphere-2022-157
Preprint. Discussion started: 26 April 2022

Short summary. Wolverine habitat inferred using a snow threshold differed for three different spatial representations of snow. These differences were annually repeatable and based on the volume of snow and the elevation of the snow line. While habitat was most influenced by winter meteorological conditions, our results show that studies applying thresholds to environmental datasets should report uncertainties stemming from different spatial resolutions and uncertainties introduced by the thresholds themselves.

Interactions between thresholds and spatial discretizations of snow: insights from wolverine habitat assessments in the Colorado Rocky Mountains

Justin M. Pflug[1,a,b], Yiwen Fang[2], Steven A. Margulis[2], Ben Livneh[1,3]

[1]Cooperative Institute for Research in Environmental Science (CIRES), University of Colorado, Boulder, CO, 80309, USA
[2]Department of Civil and Environmental Engineering, University of California, Los Angeles, CA, 90095, USA
[3]Department of Civil, Environmental and Architectural Engineering, University of Colorado, Boulder, CO, 80309, USA
[a]now at: Hydrological Sciences Laboratory, NASA Goddard Space Flight Center, Greenbelt, MD, 20771, USA
[b]now at: ESSIC, University of Maryland, College Park, College Park, MD, 20742, USA

Correspondence to: Justin M. Pflug (jpflug@umd.edu)

Abstract. Thresholds can be used to interpret environmental data in a way that is easily communicated and useful for decision making purposes. However, thresholds are often developed for specific data products and time periods, changing findings when the same threshold is applied to datasets or periods with different characteristics. Here, we test the impact of different spatial discretizations of snow on annual estimates of wolverine habitat in the Colorado Rocky Mountains, defined using a snow water equivalent (SWE) threshold (0.20 m) and threshold date (15 May) from previous habitat assessments. Annual wolverine habitable area (WHA) was thresholded from a 36-year (1985 – 2020) snow reanalysis at three different spatial discretizations: 1) 480 m grid cells, 2) 90 m grid cells, and 3) 480 m grid cells with implicit representations of subgrid snow spatial heterogeneity. Relative to the 480 m grid cells, 90 m grid cells resolved shallower snow deposits on slopes between 3050 and 3350 m elevation, decreasing WHA by 10%, on average. In years with warmer and/or drier winters, grid cells with subgrid representations of snow heterogeneity increased the prevalence of 15 May snow deposits that exceeded the 0.20 m SWE threshold, even within grid cells where mean SWE was less than the threshold. These simulations increased WHA by upwards of 30% in low snow years, as compared to simulations without subgrid snow heterogeneity. Despite WHA sensitivity to different snow spatial discretizations, WHA was controlled more by annual variations in winter precipitation and temperature. However, small changes to the SWE threshold ($\pm$ 0.07 m) and threshold date ($\pm$ 2 weeks) also affected WHA by as much as 82%. Across these threshold ranges, WHA was approximately 18% more sensitive to the SWE threshold than the threshold date. However, the sensitivity to the threshold date was larger in years with late spring snowfall, when WHA depended greatly on whether the date SWE was thresholded was before, during, or after spring snow accumulation. Our results demonstrate that snow thresholds are useful but may not always provide a complete picture of the annual variability in snow-adapted wildlife habitat. Studies thresholding spatiotemporal datasets could be improved by including 1) information about the fidelity of thresholds across multiple spatial discretizations, and 2) uncertainties related to ranges of realistic thresholds.

1. Introduction

Generalizing environmental data using thresholds can present information in a way that is more easily understood, communicated, and applied for decision-making purposes. Conceptually, thresholds are static constraints intended to partition the areas, timing, and/or prevalence of data greater or less than some scientifically or managerially relevant limit. In the field of snow science, thresholds are used to classify snow cover and snow absence from remotely-sensed observations (Dozier, 1989; Hall and Riggs, 2007; Sankey et al., 2015), partition snow accumulation and snowmelt seasons (Cayan, 1996; Hamlet et al., 2005; Mote et al., 2005; Serreze et al., 1999), and parameterize modeled processes like snow-layer formation and merging (e.g., Clark et al., 2015; Liston and Elder, 2006; Wigmosta et al., 2002), rain and snow precipitation partitions (Auer, 1974; Harder and Pomeroy, 2013), and snow

https://doi.org/10.5194/egusphere-2022-157
Preprint. Discussion started: 26 April 2022

holding capacity on steep slopes (Bernhardt and Schulz, 2010). Thresholds are also used to identify drought conditions in snow-dominated watersheds (Dierauer et al., 2019; Harpold et al., 2017; Heldmeyer et al., *In Review*), and the associated "decision trigger" and "tipping point" thresholds that determine water use and allocation in regulated basins (Herman and Giuliani, 2018; Kwadijk et al., 2010; Shih and ReVelle, 1995). However, despite widespread use, thresholds are often developed for specific applications, and over short time intervals, decreasing the likelihood that a threshold developed for one purpose could be applied in an identical manner to different periods of time, or to environmental products with different characteristics (Härer et al., 2018; Jennings et al., 2018; Maher et al., 2012; Pflug et al., 2019).

Here, we focus on snow thresholds that have been used increasingly over the past decade to identify regions with conditions suitable for the survival of snow-adapted wildlife. Many studies use thresholds that focus on snow characteristics like snow depth, snow cover, snow density, snow water equivalent (SWE), and snowmelt season snow persistence, which can be important for denning, migration, and food-availability for species like North American wolverines (*gulo gulo luscus*), polar bears (*Ursus maritimus*), and Dall sheep (*Ovis dalli dalli*) (Barsugli et al., 2020; Durner et al., 2013; Liston et al., 2016; Mahoney et al., 2018; McKelvey et al., 2011; Sivy et al., 2018). However, few studies simulate snow at spatial resolutions that correspond to the features that drive snow habitat. For instance, wolverines rely on snow drifts for maternal and natal denning. These drifts often form alee of obstructions near the forest edge and in talus fields (e.g., Fig. 1, star). Yet, few models simulate snow at den-scale spatial-resolutions (< 10 m), and represent the physical processes that control the formation of dens, like wind-redistribution, preferential deposition, avalanching, and microtopographic shading. This is particularly the case for species status assessments which often attempt to quantify wildlife habitat at large regional extents where high-resolution snow simulations with complex physical processes would be computationally prohibitive. Thresholds are therefore used to facilitate the relationship between a coarser-resolution representation of snow, and the finer-scale feasibility of wildlife habitat. The validity of this approach is debated (e.g., Araújo and Peterson, 2012; Barsugli et al., 2020; Boelman et al., 2019; Bokhorst et al., 2016; Copeland et al., 2010; Magoun et al., 2017). For example, coarser-scale representations of snow may resolve the larger-scale meteorological influences on habitat availability, but coarser-scale representations of snow likely overlook the smaller-scale refugia that could continue to support habitat, even with future changes to climate.

This manuscript builds on a study from Barsugli et al. (2020), which used physically-based simulations to identify wolverine habitable areas using SWE thresholds, including a SWE threshold (0.20 m) from known denning locations on a static date (15 May) corresponding to the tail end of the maternal denning period (Copeland et al., 2010; Heim et al., 2017; McKelvey et al., 2011; USFWS, 2018). Barsugli et al. (2020) found that, relative to previous studies that used ~10 km products (Laliberte and Ripple, 2004; McKelvey et al., 2011), snow simulations at 250 m resolution were able to better resolve SWE persistence, and increased habitat, on shaded north-facing slopes. 250 m simulations also increased the overall prevalence of snow that could support Wolverine habitat, both in current and future climates, over Colorado and Montana Rocky Mountain domains.

Here, we extend the findings from Barsugli et al. (2020), testing the difference in wolverine habitat defined using thresholds (0.20 m SWE on 15 May) and a historic snow reanalysis with different spatial discretizations (Fig. 1). These discretizations include: 1) discrete 480 m grid cells (D480), 2) discrete 90 m grid cells (D90), and 3) 480 m grid cells with implicit representations of subgrid SWE spatial heterogeneity (S480). These discretizations straddle the 250 m resolution used by Barsugli et al. (2020) and include both discrete (D480 and D90) and implicit (S480) representations of snow distribution. These reanalyses, which combine snow modeling and remotely-sensed observations of snow cover (more in Sect. 2.2), also resolve snow volume and distribution in mountain terrain significantly better than more common modeling approaches (*Pflug et al., In Review* ;Yang et al., 2021). We focus over the same Colorado Rocky Mountain domain used by Barsugli et al. (2020) over a longer period of 36 years, spanning 1985 to 2020. We ask: **1) how does the spatial discretization of snow influence estimates of wolverine habitable area? and 2) is the sensitivity of habitat to different snow spatial discretizations greater or smaller than habitat sensitivity to interannual changes in winter climatic conditions?** We also identify the spatial locations and causes of the greatest differences in thresholded wolverine habitat, and evaluate sensitivities to small uncertainties in both SWE thresholds (± 0.07 m) and threshold dates (± 2 weeks). More generally, this study highlights shortcomings, opportunities, and tradeoffs to thresholding spatial snow products, and serves as a roadmap for future wildlife habitat assessments.

https://doi.org/10.5194/egusphere-2022-157
Preprint. Discussion started: 26 April 2022

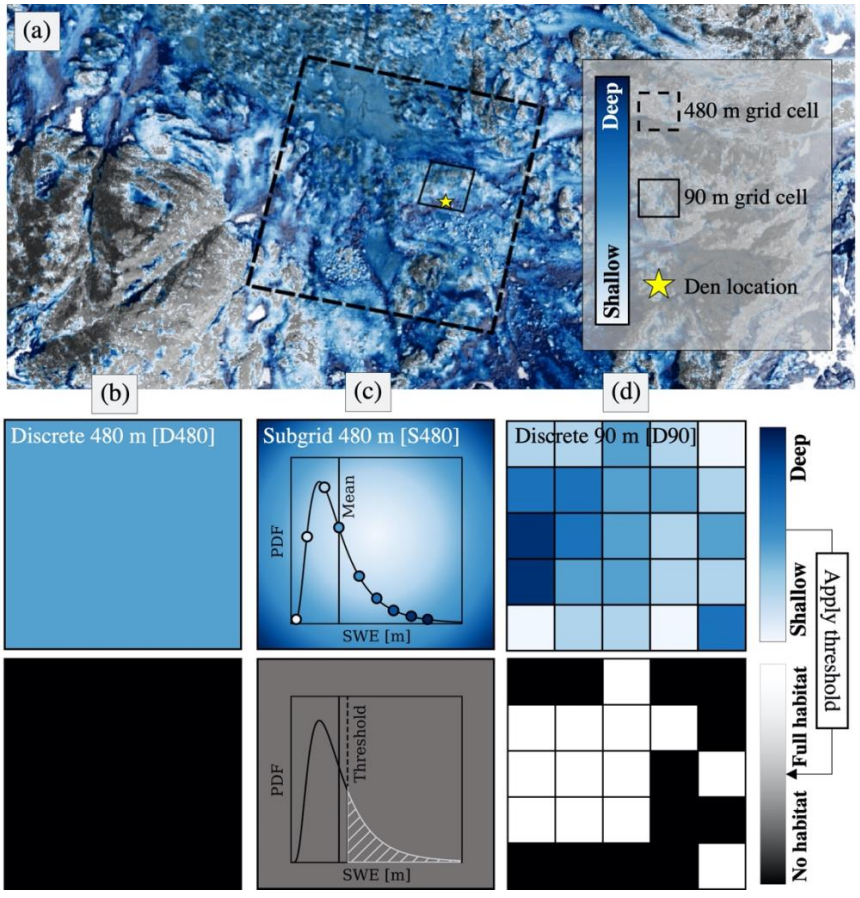

Figure 1. SWE spatial heterogeneity inferred from airborne lidar at 1 m resolution, compared to 480 and 90 m grid cells, and a point (star) with a snow drift suitably deep for wolverine denning (a). SWE is simulated in this study using three different spatial discretizations: 480 m discrete grid cells (column b), 480 m grid cells with subgrid SWE heterogeneity (column c), and 90 m discrete grid cells (column d). Wolverine habitat (bottom row) is defined for each discretization on 15 May using a 0.20 m SWE threshold. Thresholded habitat for discrete grid cells (b and d) are binary (no habitat or full habitat), while habitat for the subgrid discretization (c) is defined by the fraction of the grid cell with SWE exceeding the threshold (white hatching)

2. Domain and Data

2.1. Domain

We focused this work over Rocky Mountain National Park in Colorado state (Fig. 2). This domain is home to several snow-adapted wildlife species, and has been included in wolverine habitat assessments (Barsugli et al., 2020; McKelvey et al., 2011; USFWS, 2018). Barsugli et al. (2020) estimated most of the terrain supportive of wolverine habitat in this region to be between 2700 and 3600 m of elevation. Although few wolverines have been sighted here, this region is of potential interest for species reintroduction. More information about wolverine habitat can be found in the U.S. Fish and Wildlife Service species status assessment (USFWS, 2018).

The Rocky Mountain National Park domain contained several snow observations (Fig, 2). These observations included 28 snow telemetry (SNOTEL) stations, deployed and managed by the National Resources and Conservation Service. These stations use snow pillows to measure the weight of snowpack and resulting SWE. A distributed lidar observation of snow depth in southernmost portion of the domain was also collected by the National

https://doi.org/10.5194/egusphere-2022-157
Preprint. Discussion started: 26 April 2022

Center for Airborne Laser Mapping in May 2010. These observations were used to assess the accuracy of the SWE reanalysis discussed in Sect. 2.2.

2.2. SWE Reanalyses

SWE was calculated over the Rocky Mountain domain (Figure 2) using a satellite-era (water years 1985 – 2020) probabilistic snow reanalysis (Margulis et al., 2019, 2016, 2015) performed at 3 arcseconds (~90 m) and 16 arcseconds (~480 m). This reanalysis was generated at each individual grid cell using an ensemble of simulations forced by the Modern-Era Retrospective analysis for Research and Applications, Version 2 (MERRA-2; Gelaro et al., 2017), and simulated using the simplified Simple Biosphere Model, Version 3 (Xue et al., 1991) coupled with the Liston (2004) snow depletion curve. The forcing dataset was downscaled to the simulation grid (Girotto et al., 2014; Margulis et al., 2015) before running the land surface model. Model ensemble members were provided different 1) precipitation multipliers (influencing total snow mass), 2) snow albedo decay functions (influencing the rate of snow ablation), and 3) parameterizations of subgrid snow spatial variability (influencing subgrid snow cover during snowmelt), among other parameters. The reanalysis then reweighted the ensemble members to most-heavily favor those that matched the satellite-observed snow cover disappearance throughout the snowmelt season. Relative to independent SNOTEL observations of SWE between 1985 and 2020 in the Rocky Mountain domain, the reanalysis exhibited a coefficient of correlation of 0.82 (not pictured). On average, the reanalysis was biased low relative to the snow pillow observations by approximately 23%. However, this could be attributed to the location of SNOTEL observations in forested clearings (Fig. 2a) which typically have SWE deeper than the terrain covered by the 480 and 90 m pixels (Livneh et al., 2014; Pflug et al., *In Review*).

For the 480 m grid cells with subgrid snow variability (Fig. 1c, S480), the heterogeneity of SWE was estimated using a method developed by Liston (2004). This method assumes that the subgrid heterogeneity of SWE accumulation is lognormally distributed, and is dictated by a *time-constant* coefficient of variation (CoV),

$$CoV = \frac{\sigma}{\mu}, \quad (1)$$

where μ is the grid cell mean SWE and σ is the standard deviation of the SWE within that grid cell. The CoV of subgrid SWE accumulation (Fig. 2b and 2c) was determined for each 480 m grid cell using the most common pattern of SWE accumulation from the overlapping 90 m reanalysis grid cells (Fig. 1d) between 1985 and 2020 (detailed further in Text S1). In Sect. 3.1, we discuss how CoV was used to estimate the temporal evolution of subgrid SWE heterogeneity.

https://doi.org/10.5194/egusphere-2022-157
Preprint. Discussion started: 26 April 2022

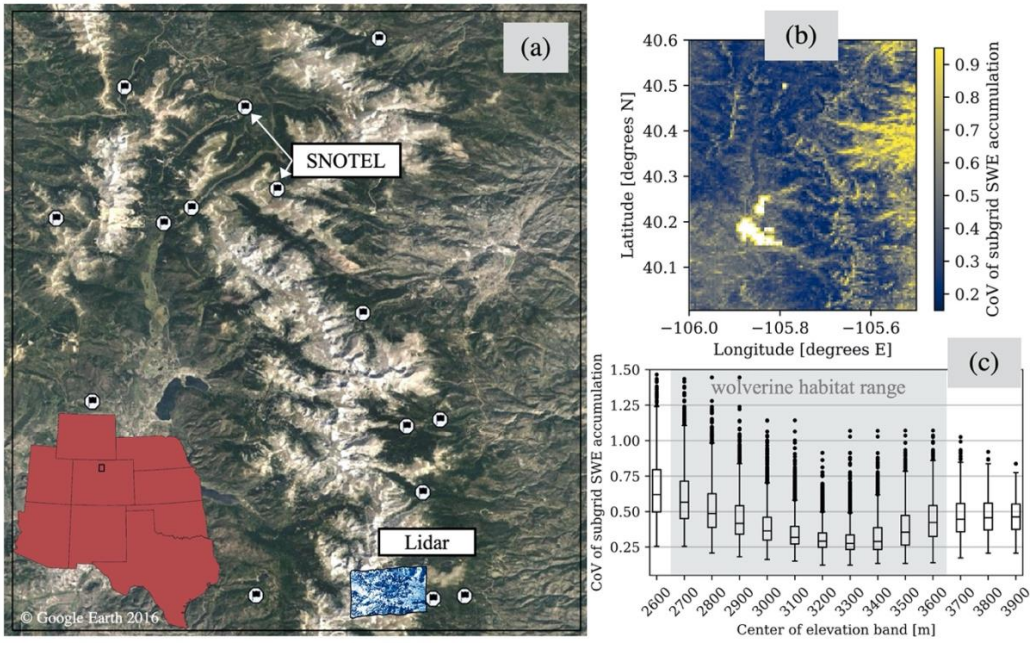

Figure 2. Rocky Mountain National Park study domain. The location of SNOTEL observations and lidar snow depth observations are superimposed in the terrain map (a). The 480 m coefficient of variation of subgrid SWE accumulation is shown both spatially (b) and across 100 m elevation bands (c).

3. Methods

The methods evaluate the impacts of snow spatial discretizations and winter climatic conditions on assessments of total area suitable for wolverine habitat. We investigated three different spatial discretizations; two discretizations using more common discrete representations of snow, and one with an implicit representation of subgrid snow heterogeneity (see Sect. 3.1). For each, annual wolverine habitable area (WHA) was calculated using a static SWE threshold (0.20 m) on a static spring date (15 May) (Sect. 3.2). Finally, we partitioned years with winter precipitation magnitude and precipitation phase anomalies, relative to average conditions from the snow reanalysis between water years 1985 and 2020 (see Sect. 3.3). These anomalies were used to examine whether winter climatic conditions or model representations of snow spatial distribution most-influenced estimates of annual wolverine habitat.

3.1. Subgrid SWE evolution

The temporal evolution of subgrid SWE heterogeneity was estimated for 480 m grid cells (Fig. 1, S480) using methods developed by Liston (2004) (Fig. 3). Provided the reanalysis grid cell mean SWE (μ) from a discrete 480 m grid cell, and a CoV of subgrid SWE accumulation (Fig. 2b), the probability distribution of subgrid SWE for that grid cell ($f(SWE)$) was calculated using a lognormal distribution,

$$f(SWE) = \left(\frac{1}{SWE\zeta\sqrt{2\pi}}\right) exp\left[-\frac{1}{2}\left[\frac{\ln(SWE) - \lambda}{\zeta}\right]^2\right], \quad (2)$$

$$\lambda = \ln(\mu) - \frac{1}{2}\zeta^2, \quad (3)$$

https://doi.org/10.5194/egusphere-2022-157
Preprint. Discussion started: 26 April 2022

$$\zeta^2 = \ln(1 + CoV^2). \quad (4)$$

Figure 3b demonstrates the subgrid distribution of SWE in two winter periods (t_a^1 and t_a^2) assuming the mean SWE evolution from Fig. 3a, a CoV of 0.50, and Eq. 2 – 4.

In the snowmelt season, the Liston (2004) methodology assumes spatially-uniform snowmelt, causing snow disappearance first in locations with thinner SWE, and last in locations with deeper SWE. This can be conceptualized as taking the subgrid distribution of snow at peak SWE (Fig. 3b, t_2^a), and adjusting it downwards by a constant amount to reflect spatially-uniform melt (SWE_m) (Fig. 3c). In doing so, snow would only exist for portions of the gridcell where $f(SWE)$ at peak SWE was greater than SWE_m. Therefore, the fractional snow-covered area (fSCA) of the grid cell could be calculated from the fraction of the distribution ($f(SWE)$) with SWE greater than SWE_m,

$$fSCA = \int_{SWE_m}^{\infty} f(SWE) dSWE. \quad (5)$$

Since SWE_m can exceed the amount of SWE that exists in some locations at peak SWE timing, and since SWE cannot be less than 0 m (snow-absent), the change in gridcell mean SWE (μ) throughout snowmelt will not necessarily equal SWE_m. Rather, μ throughout the snowmelt season can be calculated from the expected value of the melt-shifted distribution (Fig. 3c),

$$\mu = \int_{SWE_m}^{\infty} [SWE - SWE_m] f(SWE) dSWE. \quad (6)$$

In this study, we were provided μ from the reanalysis at each 480 m grid cell and daily timestep. Using the CoV (Fig. 2b) and maximum annual μ at each grid cell, we calculated the SWE distribution (Eq. 2) for each grid cell at peak SWE timing. Then, using a Newton-Raphson solver, we solved the SWE_m for each grid cell that caused μ from Eq. 6 to match μ from the 480 m reanalysis grid cell on 15 May.

The Liston (2004) subgrid SWE parameterization discussed above operates under several assumptions. Like many other studies (e.g., Donald et al., 1995; Helbig et al., 2021; Jonas et al., 2009), Eq. 2 assumes that the distribution of snow accumulation at scales finer than the grid cell resolution can be represented by a lognormal distribution. We tested this assumption by evaluating the distribution of 1 m lidar snow depth observations (Fig. 2a) that fell within 480 m grid cells. The Kolmogorov-Smirnov (KS) statistic, or maximum difference between cumulative distribution functions, was used to test how well different theoretical distributions (e.g., normal, lognormal, gamma, Rayleigh, chi, etc.) matched the lidar-observed snow depth distributions. The KS statistic for the lognormal distribution (Eq. 2) was 0.12 ± 0.05, and was significantly worse (greater than 0.22) when comparing the observed lidar distributions versus other common distributions, like normal and gamma distributions. While not perfect, these results showed that subgrid snow heterogeneity was approximated best by lognormal distributions. The Liston (2004) subgrid methodology also assumed that the CoV of subgrid SWE accumulation was constant, resulting in a linear increase in SWE variability (standard deviation) with mean SWE throughout the snow accumulation season (Fig. 3b). While we lacked validation data to test this, this assumption is the basis for other modeling approaches, which scale snow input using information from historic snow accumulation patterns (Liston, 2004; Luce et al., 1998; Pflug et al., 2021; Vögeli et al., 2016). Finally, although subgrid snowmelt is not spatially-uniform, melt-season snow heterogeneity is often modeled well by assuming uniform snowmelt. This is due to the outsized influence of snow accumulation spatial heterogeneity on snowmelt onset timing and snowmelt rates (Egli et al., 2012; Luce et al., 1998; Lundquist and Dettinger, 2005; Pflug and Lundquist, 2020). Readers should refer to Liston (2004) for more information about the subgrid snow methodology described in this section.

https://doi.org/10.5194/egusphere-2022-157
Preprint. Discussion started: 26 April 2022

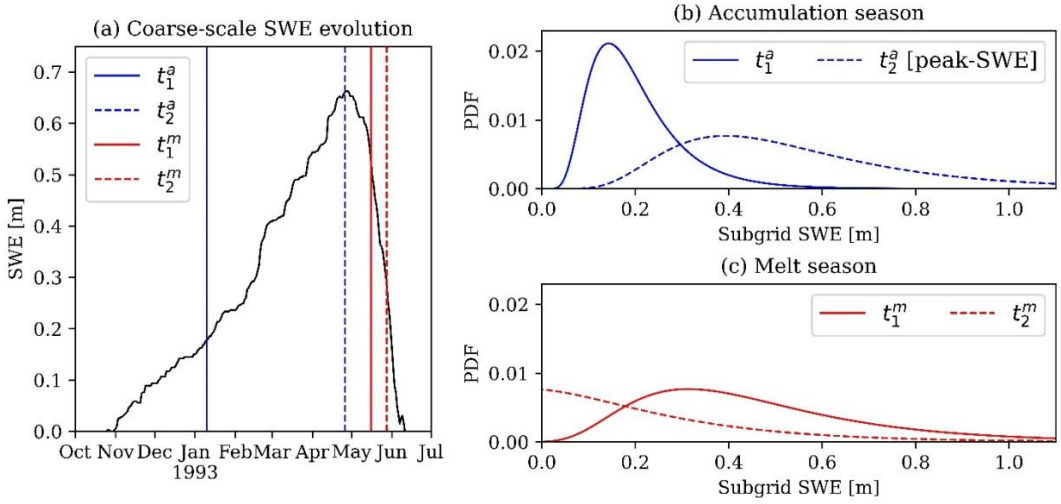

Figure 3. An example of the Liston (2004) subgrid SWE parameterization assuming CoV = 0.5, and SWE evolution for a 480 m grid cell in a random year (panel a). Subgrid SWE distributions are shown for two times (*t*, subscripts 1 and 2) in the accumulation (superscript a) and melt (superscript m) seasons (panels b and c, respectively). The timing of each date corresponds to the matching vertical bar in panel a.

3.2. Thresholding wolverine habitable area

The area that could support wolverine habitat was calculated for each of the discretizations in each year using a SWE threshold of 0.20 m on 15 May, in accordance with previous studies (e.g., Barsugli et al., 2020; Copeland et al., 2010; McKelvey et al., 2011). For the 480 and 90 m discrete reanalyses (D480 and D90), each cell's habitable fraction (HF) was classified as fully-habitable (HF = 1.0) or uninhabitable (HF = 0.0) if the 15 May grid cell mean SWE was greater than or less than 0.20 m, respectively. For the 480 m simulation with subgrid snow heterogeneity (S480), HF was calculated for each grid cell using:

$$HF = \int_{SWE_m+\alpha}^{\infty} f(SWE)dSWE, \quad (5)$$

which represented the portion of the cell's SWE distribution greater than the SWE threshold ($\alpha = 0.20$ m). WHA was calculated for each discretization as the sum of HF (in space), multiplied by grid cell area.

Relative to HF calculated from a discrete 480 m grid cell, HF calculated over the same area from the finer-scale discretizations (S480 and D90) could have one of four possible relationships. First, the mean SWE of the D480 grid cell, and the finer-scale distribution of SWE (S480 and D90), could both be entirely greater than the 0.20 SWE threshold. This results in a fully-habitable area (HF = 1.0) for all discretizations (Fig. 4a). HF would also agree in regions where all discretizations have SWE below 0.20 m (Fig. 4d), resulting in no habitat (HF = 0.0). The scenarios shown in Fig. 4b and Fig. 4c are where HF is sensitive to the discretization. Figure 4b shows a scenario where the coarse-scale D480 mean SWE is sufficiently deep enough to be classified as fully-habitable (SWE > 0.20 m), even though some portion of that grid cell contains SWE that is shallower than the SWE threshold. Therefore, using a finer-scale discretization would result in a net loss in habitat relative to the D480 discretization, the magnitude of which is shown by the red hatching in Fig. 4b. Of course, the opposite could be true for instances where coarse-scale mean SWE falls below the 0.20 m SWE threshold, thereby underestimating habitat relative to finer-scale representations that resolve some deeper snow deposits (Fig. 4c, blue hatching). Since the three reanalysis discretizations are provided identical meteorological forcing, and resolve similar SWE (within 1%), the degree to which the scenarios shown in Fig. 4b and 4c occur were the drivers of habitat differences.

https://doi.org/10.5194/egusphere-2022-157
Preprint. Discussion started: 26 April 2022

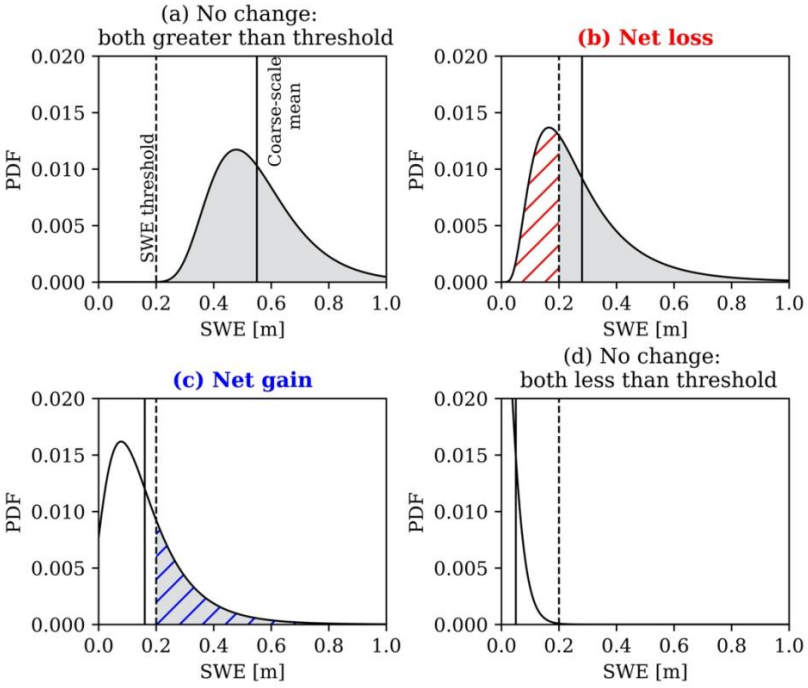

Figure 4. Conceptual portrayal of the similarities (a and d) and differences (b and c) in wolverine habitable fraction for a 480 m discrete grid cell (vertical solid line) and a finer-scale representation (distribution) of SWE over the same area. The vertical dashed lines represent the 0.20 m SWE threshold. Shaded areas show the portion of the distribution with SWE greater than the threshold. Hatched areas demonstrate differences in habitat between the coarser and finer-scale discretizations of SWE.

3.3. Categorizing winter climate anomalies

To determine WHA sensitivity to different climatic conditions, we identified years from the reanalysis with anomalous winter precipitation magnitude and phase (rain versus snow). Here, winter is defined by periods between October 1st and the date of domain peak SWE volume. Following work from Heldmeyer et al. (*in review*), we used basin average cumulative winter precipitation and the fraction of the winter precipitation that fell as snow (both from the reanalysis) as indices for winter precipitation magnitude and the temperature at which precipitation fell. Using a percentile, we separated years that fell at least that far from the 1985 – 2020 median precipitation magnitude and fraction of snow precipitation. In doing so, we partitioned years with wet, dry, cold, and warm winter anomalies. We did this separation using a range of percentiles until the statistical difference (measured using the Mann-Whitney u-test) in D480 WHA was maximized between the years with different climatic conditions (warm, cold, wet, dry, and typical). To avoid spurious results, this percentile was also adjusted to ensure that each anomaly included at least 6 years. This approach maximized the difference in interannual WHA as a function of different winter climatic conditions. This was then used as the baseline to compare how much more or less sensitive WHA was to the different SWE spatial discretizations.

4. Results

The spatial variability of subgrid SWE accumulation (Sect. 2.2 and Text S1) had a relationship with the terrain (Fig. 2b and 2c). Over low-elevation forested grid cells (< 2800 m), SWE accumulation variability was large relative to the smaller amounts of snow, resulting in large CoV (typically between 0.50 and 0.80). On mid-elevation slopes (2800 – 3300 m), where winter snowmelt was less common, CoV tended to be smaller (approximately 0.30, on average). However, CoV increased again at higher elevations (> 3300 m), and particularly on the leeward side of peaks. This was expected given the more extreme terrain and increased spatial variability of snow from wind-drifting, preferential deposition, cornice formation, and avalanching.

https://doi.org/10.5194/egusphere-2022-157
Preprint. Discussion started: 26 April 2022

The difference in wolverine habitable area (WHA) was maximized between 1) warm and cold years, and 2) wet and dry years, that had winter precipitation magnitude (Fig. 5a, x-axis) and precipitation phase (Fig. 5a, y-axis) that fell above the 77th and below the 23rd percentiles (±27th percentile from the median). These anomalies had impacts on the annual evolution of SWE and snow-covered area (Fig. 5b and Fig. 5c). On average, as compared to years with normal winter precipitation magnitude and phase (Fig. 5a, white region), cold years and wet years had peak SWE volume that was 23% and 28% greater, respectively. This was opposed to warm years and dry years, with peak SWE volume that was 21% and 31% smaller, on average, than typical water years. The timing of peak-SWE was driven most by the magnitude of winter precipitation. In fact, average peak-SWE timing was 28 days later for wet years than dry years. Snow disappearance timing (snow-covered area < 200 km^2) was also 21 days later for wet years than dry years. Statistically, the timing of snow disappearance, crucial for wolverine denning habitat, was explained well by the peak-SWE volume (r = 0.82) and the date of peak-SWE (r = 0.63), both of which were influenced more by winter precipitation magnitude than temperature.

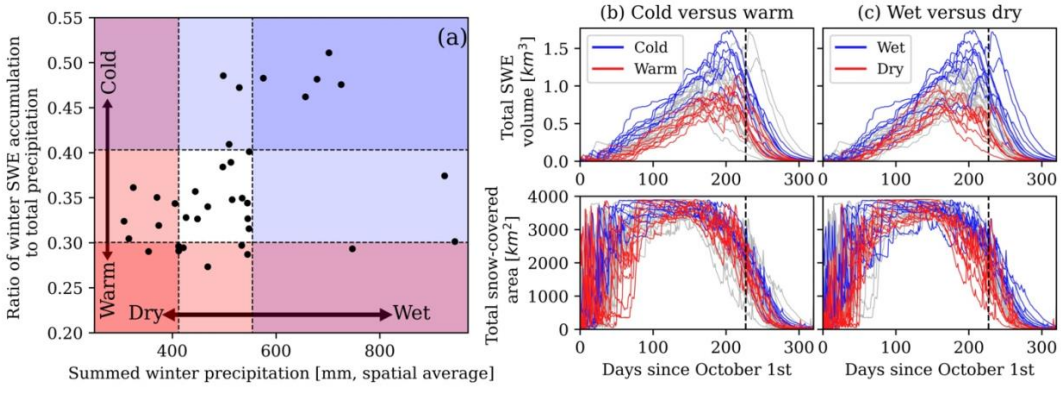

Figure 5. Annual climatic conditions grouped into anomaly categories based on winter precipitation magnitude (a, horizontal-axis) and precipitation phase (a, vertical-axis) outside the 23rd and 77th percentiles (a, dashed lines). The annual evolution of SWE volume and snow cover are compared for warm versus cold (column b) and wet versus dry years (column c). Vertical dashed lines in columns c and d indicate 15 May.

In all years except dry 2002, WHA was smaller for the D90 discretization than the D480 discretization (Fig. 6). This resulted in a 10% reduction to the 36-year median WHA (Fig. 6b). The WHA differences between the D480 and S480 discretizations varied more on an annual basis. For years with D480 WHA less than 1000 km^2, S480 discretizations increased WHA by up to 30%, 11% on average. However, in years with WHA greater than 1000 km^2, S480 WHA was approximately 3% smaller, on average, than D480 WHA. In short, the S480 discretization tended to have less-dramatic annual swings in WHA than the D480 discretization. The causes of these WHA disagreements are discussed in Sect. 5.1. Despite the interannual differences in D480 and S480 WHA, the 36-year median WHA for these discretizations agreed to within 1% (Fig. 6b).

https://doi.org/10.5194/egusphere-2022-157
Preprint. Discussion started: 26 April 2022

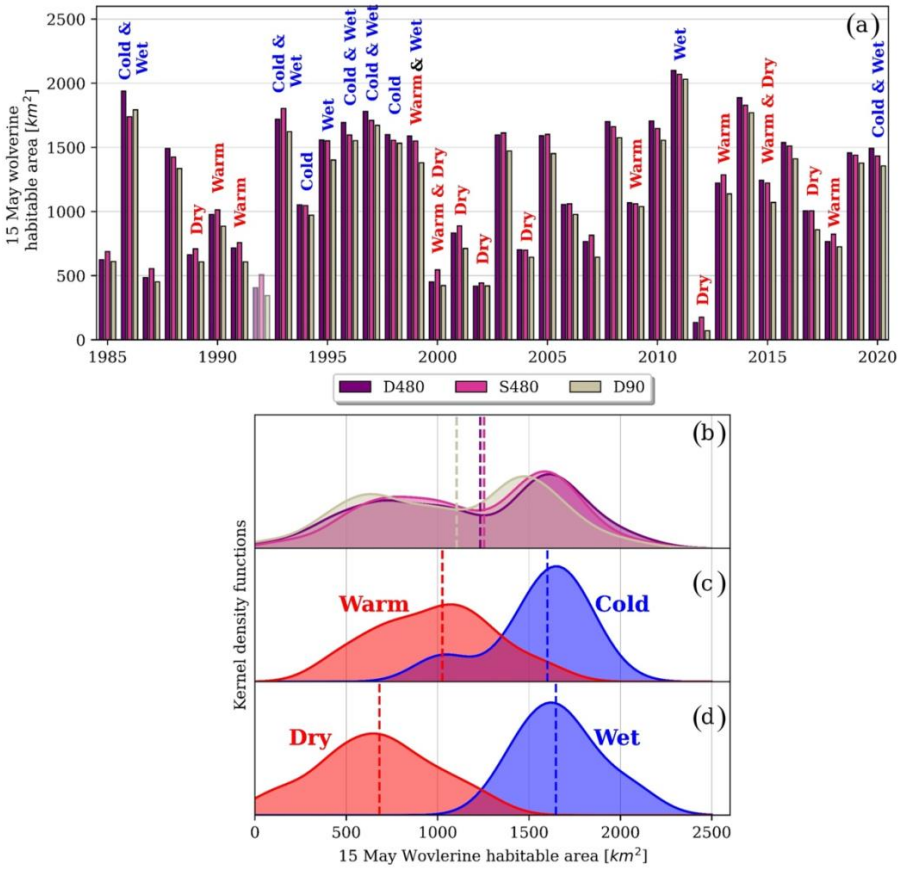

Figure 6. 15 May wolverine habitable area compared annually for three different spatial discretizations (a). Lower panels show the kernel distributions for the data in panel a, separated based on the spatial discretization (b), temperature anomalies (c), and precipitation anomalies (d). The medians of each distribution are shown by the vertical dashed lines (b – d). The data in panels c and d include data from all three spatial discretizations. The data from WY1992 (a, faded bars) exhibited artifacts, and was excluded from the kernel distributions (b-d).

Even though WHA was sensitive to different spatial discretizations (Fig. 6b), WHA across the 36-year period was not statistically different between any of the three discretizations ($p > 0.48$). Conversely, the difference in 15 May WHA was significantly larger between the years with different winter climate anomalies (Fig. 6c and 6d). Differences in WHA between years with anomalously warm and cold conditions were statistically significant ($p = 1 \times 10^{-5}$), and even more different between the years with dry and wet conditions ($p = 1 \times 10^{-8}$). While WHA was not statistically different between cold and wet years ($p = 0.34$), the distribution of WHA in dry years was significantly smaller than the distribution of WHA in warm years ($p = 0.001$), showing that WHA was more sensitive to conditions that reduced snow habitat, like warm and dry anomalies.

The results from Fig. 6 suggest that changes in WHA across annual periods of differing climatic conditions, or across future periods with expected changes in climate (e.g., Barsugli et al., 2020) should be informative from a species status assessment perspective, regardless of the snow spatial discretizations that we tested here. However, as noted above, S480 discretization increased WHA by 11% on average in low snow years, with increases as large as 30% for individual years. These low snow years often corresponded with drier and/or warmer winter conditions, the latter of which are expected in the future. For example, the average air temperature during December, January, and February precipitation events during warm years in the reanalysis record was approximately 0.8° higher than winter precipitation events in typical years. These conditions are consistent with what is projected for this region by 2055

https://doi.org/10.5194/egusphere-2022-157
Preprint. Discussion started: 26 April 2022

(Eyring et al., 2016; Scott et al., 2016). This suggests that the disparity between habitat inferred from discrete grid cells, and grid cells with subgrid snow heterogeneity, could be of greater importance for future snow habitat assessments. Additionally, using WHA as the sole metric for evaluating differences in annual wolverine habitat may oversimplify the degree to which static thresholds and different spatial discretizations interact. For instance, WHA inferred on a static date (15 May) compares very different regimes of the snow season. as wet years had peak SWE timing, and snowmelt season onset, that was 21 days later than typical snow seasons (Fig. 5). Since shallower snow melts more readily than deeper snow (provided the same energy), comparing WHA on a static date in years with very different conditions neglects the different rates of habitat depletion for a few days on either side of the date threshold. These issues are investigated more in Sect. 5.

5. Discussion

In this section we diagnose the locations and causes for habitat disagreements between the three spatial discretizations of snow (Sect. 5.1) and investigate how the use of a static SWE threshold and threshold date, may obscure the picture of interannual changes to snow habitat availability (Sect. 5.2). Using these findings, we discuss how information provided from multiple spatial discretizations could provide information about the fidelity and uncertainty of thresholds, as well as the interactions and tradeoffs between spatial discretizations and thresholds, both in context for assessing snow-adapted wildlife habitat, and more broadly for other environmental studies (Sect. 5.3).

5.1. Spatial habitat differences

The spatial difference in habitable fraction (HF) between the three discretizations had annually similar patterns, with the largest differences at locations where the domain had SWE that was near the 0.20 m SWE threshold. This was illustrated in Fig.7, where the greatest number of HF disagreements on 15 May 2008 were focused between approximately 2800 and 3200 m of elevation. Relative to the D480 discretization, the S480 discretization tended to increase habitat in grid cells at lower elevations where mean SWE was less than the SWE threshold, but some portion of the grid cell had SWE deep enough to support habitat (e.g., Fig. 4c). The opposite effect occurred at higher elevations where mean SWE exceeded the SWE threshold, but the lower-tails of the S480 SWE distributions were below the threshold (e.g., Fig. 4b). As a result, the S480 discretization had a more-gradual increase in habitat with elevation, and a downward shift in the elevations that could support wolverine habitat (Fig. 7f). In fact, relative to the D480 discretization, the S480 discretization had 23% less interannual variability in the elevation of median habitat (Fig. S1a), or elevation at which equal WHA existed at higher and lower elevations. This was a result of the subgrid representations of SWE heterogeneity which allowed for gradual and fractional ($0.0 \leq HF \leq 1.0$) increases in HF with increases in SWE. This was opposed to the D480 discretization, which could only resolve binary HF (0 or 1 for SWE less than and greater than 0.20 m), resulting in larger topographical shifts in the annual location of wolverine habitat.

https://doi.org/10.5194/egusphere-2022-157
Preprint. Discussion started: 26 April 2022

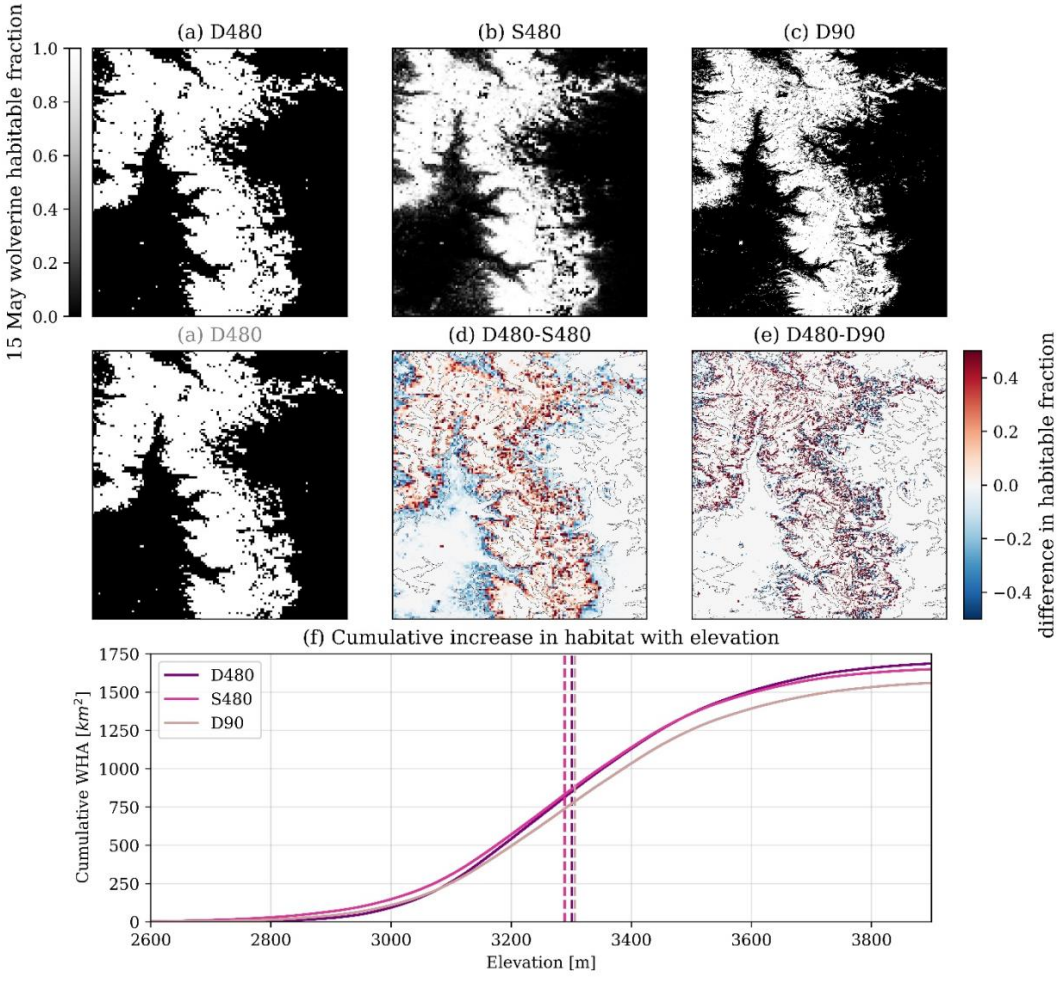

Figure 7. Spatial comparisons of habitable fractions for the three discretizations on 15 May 2008. Panel f compares the cumulative WHA (y-axis) calculated for grid cells sorted in order of increasing elevation (x-axis). Vertical dashed lines show the elevation of median habitat, or elevation at which WHA is equal for higher and lower elevations.

Relative to the D480 discretization, the D90 discretization also tended to increase HF at lower elevations. However, all years had reduced D90 HF in elevations higher than the snow line. This was the cause of the 10% reduction in D90 WHA, relative to the other discretizations (Fig. 6b). These decreases in habitat were typically located on unvegetated, exposed, and steep slopes, where it was likely that winter snow retention was decreased, snow sublimation was increased, and sloughing to lower-elevations was more common (Bernhardt and Schulz, 2010; Grünewald et al., 2014; Machguth et al., 2006). This demonstrates the utility of the observation-based reanalysis used in this study, which may have resolved thinner snow deposits on slopes with decreased snow retention and/or enhanced snow removal by processes like sloughing, both of which are among the most-difficult processes to represent with models. The D480 discretization averaged snow from surrounding areas, smoothing out thinner snow deposits resolved by the D90 discretization. Although attempting to resolve subgrid snow heterogeneity, the evolution of SWE assumed by the S480 simulation, which assumed lognormal snow accumulation and spatially-uniform subgrid snowmelt (Fig. 3), may have been less-appropriate for the areas containing these isolated thinner-snow 90 m gridcells. While the D90 discretization decreased total WHA, D90 snow cover was also patchier (Fig.

https://doi.org/10.5194/egusphere-2022-157
Preprint. Discussion started: 26 April 2022

7c), which could also influence the movement and connectivity for Wolverines (USFWS, 2018) and other snow-adapted species.

Winter precipitation magnitude and temperature influenced the volume of snow and the elevation of the snow line that existed on 15 May in each year. Since the differences in HF between the discretizations were largest at grid cells near the 0.20 m SWE threshold, often located just above the snow line, the spatial pattern of HF differences (e.g., Fig. 7) exhibited an interannually-repeatable relationship with the dry, warm, cold, and wet winter anomalies (Fig. 5). To show this, we calculated the differences in HF between all three discretizations (D480 versus S480, D480 versus D90, and S480 versus D90) in all 36 years. Then, for each 480 m grid cell, we calculated the climate anomaly that had the greatest absolute differences in HF. In other words, using the historic 36-year record, we classified the meteorological condition that resulted in the greatest uncertainty in HF across the three discretizations for each 480 m grid cell. The climate anomalies that had the greatest influence on HF uncertainties covered similar portions of the domain, with 33.7%, 20.9%, 25.2%, and 20.2% being most attributed to dry, warm, cold, and wet conditions, respectively (Fig. 8). At low elevations (2650 – 3050 m), 15 May snow typically existed only in wet years. In those years and elevations, mean SWE for the D480 and D90 discretizations often fell below the 0.20 m SWE threshold. However, the large CoVs of subgrid SWE accumulation in these elevations (Fig. 2) resulted in S480 subgrid SWE distributions with upper-tails that often exceeded 0.20 m (e.g., Fig. 4c), increasing total habitat (Fig. 8c). This was in-line with findings from Magoun et al. (2017), who noted suitable denning conditions at lower-elevations, even in instances when the surrounding terrain was predominantly snow-free.

The average differences in HF between the three discretizations were largest in cold years for elevations spanning 3050 – 3150 m, and in warm years for elevations spanning 3150 – 3350 m (Fig. 8). Across this elevation range (3050 – 3350 m), both of the 480 m discretizations (D480 and S480) estimated more habitat than the D90 discretization (Fig. 8c). However, at higher elevations (> 3350 m), wolverine habitat inferred from the discretization with subgrid snow heterogeneity (S480) approached the thinner snow deposits estimated by the 90 m discretization (Fig. 8c).

https://doi.org/10.5194/egusphere-2022-157
Preprint. Discussion started: 26 April 2022

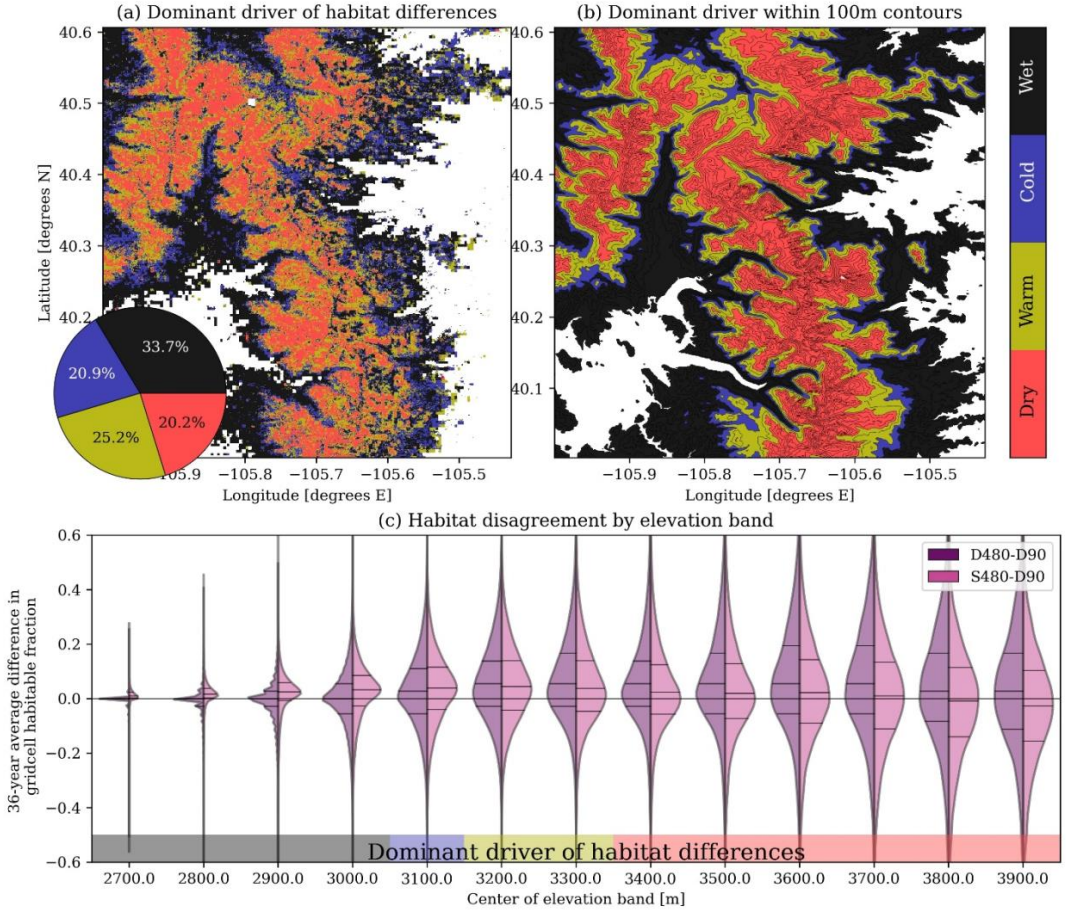

Figure 8. Winter climate anomalies that most-influenced habitat disagreements between the three discretizations (a). Panel b shows the most-common influence from panel a, for 100 m elevation bands. Using HF from the D90 discretization as a reference, the 36-year average difference in HF for the D480 and S480 simulations are shown by distributions for each 100 m elevation band (c). Lines inside the distributions show the median and interquartile range.

5.2. Threshold sensitivities

To this point, we assumed confidence in the SWE (0.20 m) and date (15 May) thresholds. However, small changes to either threshold could influence annual estimates of WHA (e.g., Copeland et al., 2010; Magoun et al., 2017). In Fig. 9, we show WHA calculated from a range of realistic SWE thresholds and threshold dates. The range of SWE thresholds (0.20 ± 0.07 m) were determined using a snow depth of 0.50 m, corresponding to observed wolverine dens (USFWS, 2018), and the 90th percentile range of 15 May snow densities from SNOTEL observations (Fig. 2a) between 1985 and 2020 ($260 - 540\ kg/m^3$). The range of threshold dates spanned a period of $\pm$ 2 weeks, corresponding to the difference in peak-SWE timing between dry and wet years (Fig. 5). This month-long time span also reflected the disparity between threshold dates and dates of observed wolverine habitat from multiple studies (Barsugli et al., 2020; Copeland et al., 2010; Magoun et al., 2017; McKelvey et al., 2011). WHA sensitivity was calculated using all combinations of SWE and date thresholds, both of which were discretized at 14 equally-spaced increments (Fig. 9, left). Then, the gradients (direction and magnitude of greatest change in WHA) were calculated from each unique combination of SWE and date thresholds. The gradients were summed using vector addition (Fig. 9, right column) to determine 1) the total rate of change in WHA with changing thresholds (arrow length), and 2) the

https://doi.org/10.5194/egusphere-2022-157
Preprint. Discussion started: 26 April 2022

degree to which WHA was sensitive to one threshold versus the other (arrow angle). This process was repeated for each discretization and year.

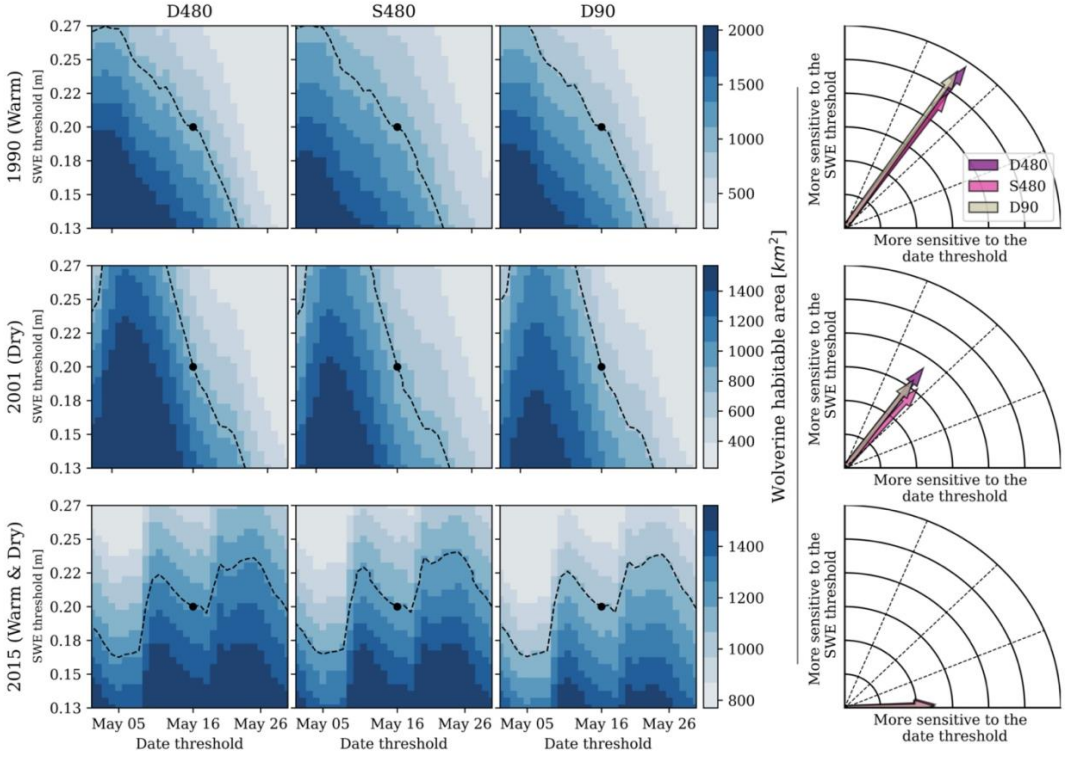

Figure 9. WHA calculated using different SWE (y-axes) and date thresholds (x-axes), for the different discretizations (columns), in three different years (rows) with very different sensitivities. WHA calculated from the default thresholds (0.20 m SWE on 15 May) is shown by the black circle. Combinations of thresholds that could reproduce the default WHA are approximated by the dashed contour. The rightmost arrows show the total direction and magnitude of WHA changes with changes in the thresholds.

WHA in warm 1990 was 18% more-sensitive to the SWE thresholds than the threshold dates (Fig. 9, top row). To put this another way, the change in WHA across a period of ± 3 days from 15 May was approximately equal to the change in WHA from adjusting the SWE threshold by ± 2.5 centimeters. This sensitivity was similar to the average threshold sensitivity from the 36-year reanalysis record (Fig. S1b). However, multiple years exhibited unique sensitivities. For example, spring snowfall between 1 May and 6 May 2001 (Fig. 9, middle row) caused WHA to both increase and decrease over the range of date thresholds (assuming a constant SWE threshold). Therefore, WHA changed based on whether the threshold date was before, during, or after the May snowfall event, buffering the degree to which habitat was influenced by the specific winter meteorological conditions that occurred in that year. This effect also occurred in 2015, when 15 May fell between two spring snowfall events (Fig. 9, bottom row). As a result, WHA tended to increase, on average, over the range of threshold dates, resulting in heightened sensitivities to the date on which habitat was evaluated. Overall, WHA varied by as much 82% between the realistic thresholds shown in Fig. 9. This was similar in magnitude to the differences in WHA between years with opposing winter climate anomalies (Fig. 6c and 6d).

In most years, the sensitivities to the thresholds were largest for the D480 simulation, and smallest for the S480 simulation (Fig. 9 and Fig. S1b). As discussed in Sect. 5.1, the S480 discretization, which represented subgrid snow distribution and fractional changes to HF with changes to the SWE threshold and threshold date, had less sensitivity to interannual changes in meteorological conditions. Similarly, small changes in the SWE threshold and threshold date changed the prevalence of snow habitat for discrete grid cells by larger amounts than the S480 discretization.

https://doi.org/10.5194/egusphere-2022-157
Preprint. Discussion started: 26 April 2022

This suggests that studies with subgrid representations of snow heterogeneity may decrease the sensitivity to SWE and date threshold uncertainties.

5.3. Threshold caveats and future suggestions

The D90 and S480 discretizations provided unique, but different advantages for estimating WHA. We believe that the upper-elevation decreases in D90 SWE and habitat on steep and unvegetated surfaces were realistic. These results were contrary to the findings from Barsugli et al. (2020), who in the same domain, found that finer-scale physically-based simulations resulted in net increases in wolverine habitat. However, this analysis used a joint model and observation-based approach (Sect. 2) that may have implicitly represented decreased snow retention and/or snow sloughing better than the physically based models used by Barsugli et al. (2020). The discretization with subgrid snow heterogeneity (S480), which is not as commonly used, had less-dramatic swings in total habitat with changes in annual winter climatic conditions (Fig. 6) and thresholds (Fig. 9). We therefore think that subgrid representations of snow are important for habitat assessments, especially given that snow deposits suitable for denning at scales of 10 m or less may occur in regions with otherwise little snow (Magoun et al., 2017).

The results of this study suggest that uncertainties provided from combinations of multiple discretizations, applied across a range of realistic thresholds, would be more informative than a single discretization and set of thresholds. For instance, SWE volume on 15 May 2015 was 10% less than the 36-year median 15 May SWE volume. However, due to spring snowfall (Fig. 9), SWE volume on 30 May 2015 was 31% greater than the 36-year median on the same date. The static 15 May threshold date thereby failed to capture the boost to wolverine habitat provided by snowfall a few days after 15 May. Multiple discretizations could also be used to identify the locations of most (e.g., Fig. 4a and 4d) and least-certain (Fig. 4b and 4c) habitat. This information could be used as the basis for identifying the locations where remote sensing or field campaigns could hone annual estimates of habitat, given that year's meteorological conditions. Altogether, differences across discretizations (e.g., Fig. 6) and threshold sensitivities (e.g., Fig. 9) could also be used to provide uncertainty bounds for WHA calculated in any given year.

Our results show that caution is warranted when combining gridded data and static thresholds. While we focus on the impact that thresholds and different snow spatial discretizations have on wolverine habitat, we expect these results to be applicable to other environmental applications. For instance, while temperature thresholds are widely used to partition rain and snow precipitation in models, temperature discretized at different spatial scales could influence the spatial variability of temperature and resulting snowfall volume thresholded across one or many snowfall events (e.g., Jennings et al., 2018; Nolin and Daly, 2006; Wayand et al., 2017). Snow cover thresholded using visible and infrared satellite observations may also require changes based on the size of the satellite pixels and the underlying topographic and vegetative characteristics (Härer et al., 2018; Pestana et al., 2019). Future studies should report the extent to which different spatial discretizations and ranges of realistic thresholds influence results. This information could be used to report the 1) uncertainty of thresholded outputs, 2) fidelity of different gridded products, and 3) the degree to which multiple spatial discretizations could be combined to improve the fidelity and transferability of results.

6. Conclusions

Wolverine habitable area (WHA) was thresholded using a published SWE threshold (0.20 m) on a threshold date (15 May) in a Colorado Rocky Mountain domain between 1985 and 2020. Results showed that WHA was statistically different ($p < 0.01$) between years with different winter precipitation magnitude (wet versus dry) and precipitation temperature (cold versus warm) anomalies. In fact, climate-driven differences in annual WHA were substantially larger than differences in WHA between snow discretized using 1) discrete 480 m grid cells, 2) 480 m grid cells with subgrid representations of SWE heterogeneity, and 3) discrete 90 m grid cells. Therefore, studies that assess changes in total habitat for species like wolverines with past and future changes in climate could be informative, regardless of the spatial discretizations tested.

Despite the sensitivity to winter climatic conditions, annual differences in spatial habitat patterns and parameter sensitivities emerged for the different discretizations. For instance, 90 m grid cells resolved thinner snow deposits in mid-to-upper elevations (approximately 3050 – 3350 m) that were not resolved by either of the 480 m discretizations, decreasing WHA by 10%, on average. Snow discretized with subgrid representations of SWE spatial heterogeneity also had less-dramatic swings in annual wolverine habitat. The simulations with subgrid SWE heterogeneity increased snow habitat by 10 – 30% in low-snow years, many of which were representative of future changes in average temperature expected over the next 50 years. Spatially, the differences in wolverine habitat between the three different snow discretizations were heightened at the grid cells that had SWE values close to the

https://doi.org/10.5194/egusphere-2022-157
Preprint. Discussion started: 26 April 2022

SWE threshold (0.20 m) on 15 May, the elevation of which was driven in large part by the winter climatic conditions. On average, wolverine habitat was 18% more sensitive to the SWE threshold than the date threshold, but had the smallest amount of sensitivity to the 480 m simulation with subgrid snow heterogeneity, which allowed for more gradual changes to wolverine habitat with small changes in SWE. This discretization also had the least amount of habitat sensitivity to interannual changes in winter climatic conditions. However, some years had late-spring snowfall events, altering the amount of wolverine habitat by up to 82% depending on whether the threshold date was before, during, or after the snowfall event.

Our results show that differences in how snow is spatially discretized can influence information generalized using thresholds. Therefore, future studies thresholding spatiotemporal environmental data should include multiple spatial discretizations and ranges of realistic thresholds to provide a more comprehensive picture of uncertainties associated with chosen thresholds and datasets. Although we used wolverine habitat as an example, we expect these results to be applicable to any study thresholding environmental data, especially for studies generalizing information at spatial scales finer than those of modeled or observed resolutions.

Code and data availability

Readers are encouraged to enquire about the most up-to-date version of the reanalysis from the principal developer, Steven Margulis. Scripts used in this manuscript are provided at https://github.com/jupflug/HABITAT-threshold_vs_discretization.

Author contributions

JP and BL designed the experiments. YF and SM provided the snow reanalysis. JP wrote the manuscript, with comments provided from all authors, and special supervision by BL.

Competing interests

The authors declare that they have no conflict of interest.

Support

This work was supported by the CIRES Visiting Fellows Program and the United States Geologic Survey (USGS) award G21AC10645.

Acknowledgements

We would like to thank and acknowledge support from current and past U.S. Fish and Wildlife Service staff, in particular, John Guinotte and Steve Torbit.

References

Araújo, M.B., Peterson, A.T., 2012. Uses and misuses of bioclimatic envelope modeling. Ecology 93, 1527–1539. https://doi.org/10.1890/11-1930.1

Auer, A.H., 1974. The Rain versus Snow Threshold Temperatures. Weatherwise 27, 67–67. https://doi.org/10.1080/00431672.1974.9931684

Barsugli, J.J., Ray, A.J., Livneh, B., Dewes, C.F., Heldmyer, A., Rangwala, I., Guinotte, J.M., Torbit, S., 2020. Projections of Mountain Snowpack Loss for Wolverine Denning Elevations in the Rocky Mountains. Earths Future 8, e2020EF001537. https://doi.org/10.1029/2020EF001537

Bernhardt, M., Schulz, K., 2010. SnowSlide: A simple routine for calculating gravitational snow transport. Geophys. Res. Lett. 37. https://doi.org/10.1029/2010GL043086

Boelman, N.T., Liston, G.E., Gurarie, E., Meddens, A.J.H., Mahoney, P.J., Kirchner, P.B., Bohrer, G., Brinkman, T.J., Cosgrove, C.L., Eitel, J.U.H., Hebblewhite, M., Kimball, J.S., LaPoint, S., Nolin, A.W., Pedersen, S.H., Prugh, L.R., Reinking, A.K., Vierling, L.A., 2019. Integrating snow science and wildlife ecology in Arctic-boreal North America. Environ. Res. Lett. 14, 010401. https://doi.org/10.1088/1748-9326/aaeec1

Bokhorst, S., Pedersen, S.H., Brucker, L., Anisimov, O., Bjerke, J.W., Brown, R.D., Ehrich, D., Essery, R.L.H., Heilig, A., Ingvander, S., Johansson, C., Johansson, M., Jónsdóttir, I.S., Inga, N., Luojus, K., Macelloni, G., Mariash, H., McLennan, D., Rosqvist, G.N., Sato, A., Savela, H., Schneebeli, M., Sokolov, A., Sokratov, S.A., Terzago, S., Vikhamar-Schuler, D., Williamson, S., Qiu, Y., Callaghan, T.V., 2016. Changing Arctic snow cover: A review of recent developments and assessment of future needs for observations, modelling, and impacts. Ambio 45, 516–537. https://doi.org/10.1007/s13280-016-0770-0

https://doi.org/10.5194/egusphere-2022-157
Preprint. Discussion started: 26 April 2022

Cayan, D.R., 1996. Interannual Climate Variability and Snowpack in the Western United States. J. Clim. 9, 928–948. https://doi.org/10.1175/1520-0442(1996)009<0928:ICVASI>2.0.CO;2

Clark, M.P., Nijssen, B., Lundquist, J., Kavetski, D., Rupp, D.E., Woods, R.A., Freer, J.E., Gutmann, E.D., Wood, A.W., Brekke, L.D., Arnold, J.R., Gochis, D.J., Rasmussen, R.M., 2015. A unified approach for process-based hydrologic modeling: 1. Modeling concept. Water Resour. Res. 51, 2498–2514. https://doi.org/10.1002/2015WR017198

Copeland, J.P., McKelvey, K.S., Aubry, K.B., Landa, A., Persson, J., Inman, R.M., Krebs, J., Lofroth, E., Golden, H., Squires, J.R., Magoun, A., Schwartz, M.K., Wilmot, J., Copeland, C.L., Yates, R.E., Kojola, I., May, R., 2010. The bioclimatic envelope of the wolverine (Gulo gulo): do climatic constraints limit its geographic distribution? Can. J. Zool. 88, 233–246. https://doi.org/10.1139/Z09-136

Dierauer, J.R., Allen, D.M., Whitfield, P.H., 2019. Snow Drought Risk and Susceptibility in the Western United States and Southwestern Canada. Water Resour. Res. 55, 3076–3091. https://doi.org/10.1029/2018WR023229

Donald, J.R., Soulis, E.D., Kouwen, N., Pietroniro, A., 1995. A Land Cover-Based Snow Cover Representation for Distributed Hydrologic Models. Water Resour. Res. 31, 995–1009. https://doi.org/10.1029/94WR02973

Dozier, J., 1989. Spectral signature of alpine snow cover from the landsat thematic mapper. Remote Sens. Environ. 28, 9–22. https://doi.org/10.1016/0034-4257(89)90101-6

Durner, G.M., Simac, K., Amstrup, S.C., 2013. Mapping Polar Bear Maternal Denning Habitat in the National Petroleum Reserve — Alaska with an IfSAR Digital Terrain Model. Arctic 66, 197–206.

Egli, L., Jonas, T., Grünewald, T., Schirmer, M., Burlando, P., 2012. Dynamics of snow ablation in a small Alpine catchment observed by repeated terrestrial laser scans. Hydrol. Process. 26, 1574–1585.

Eyring, V., Bony, S., Meehl, G.A., Senior, C.A., Stevens, B., Stouffer, R.J., Taylor, K.E., 2016. Overview of the Coupled Model Intercomparison Project Phase 6 (CMIP6) experimental design and organization. Geosci. Model Dev. 9, 1937–1958. https://doi.org/10.5194/gmd-9-1937-2016

Gelaro, R., McCarty, W., Suárez, M.J., Todling, R., Molod, A., Takacs, L., Randles, C.A., Darmenov, A., Bosilovich, M.G., Reichle, R., Wargan, K., Coy, L., Cullather, R., Draper, C., Akella, S., Buchard, V., Conaty, A., Silva, A.M. da, Gu, W., Kim, G.-K., Koster, R., Lucchesi, R., Merkova, D., Nielsen, J.E., Partyka, G., Pawson, S., Putman, W., Rienecker, M., Schubert, S.D., Sienkiewicz, M., Zhao, B., 2017. The Modern-Era Retrospective Analysis for Research and Applications, Version 2 (MERRA-2). J. Clim. 30, 5419–5454. https://doi.org/10.1175/JCLI-D-16-0758.1

Girotto, M., Margulis, S.A., Durand, M., 2014. Probabilistic SWE reanalysis as a generalization of deterministic SWE reconstruction techniques. Hydrol. Process. 28, 3875–3895. https://doi.org/10.1002/hyp.9887

Grünewald, T., Bühler, Y., Lehning, M., 2014. Elevation dependency of mountain snow depth. The Cryosphere 8, 2381–2394. https://doi.org/10.5194/tc-8-2381-2014

Hall, D.K., Riggs, G.A., 2007. Accuracy assessment of the MODIS snow products. Hydrol. Process. 21, 1534–1547. https://doi.org/10.1002/hyp.6715

Hamlet, A.F., Mote, P.W., Clark, M.P., Lettenmaier, D.P., 2005. Effects of Temperature and Precipitation Variability on Snowpack Trends in the Western United States. J. Clim. 18, 4545–4561. https://doi.org/10.1175/JCLI3538.1

Harder, P., Pomeroy, J., 2013. Estimating precipitation phase using a psychrometric energy balance method. Hydrol. Process. 27, 1901–1914. https://doi.org/10.1002/hyp.9799

Härer, S., Bernhardt, M., Siebers, M., Schulz, K., 2018. On the need for a time- and location-dependent estimation of the NDSI threshold value for reducing existing uncertainties in snow cover maps at different scales. The Cryosphere 12, 1629–1642. https://doi.org/10.5194/tc-12-1629-2018

Harpold, A., Dettinger, M., Rajagopal, S., 2017. Defining Snow Drought and Why It Matters. Eos. https://doi.org/10.1029/2017EO068775

Heim, N., Fisher, J.T., Clevenger, A., Paczkowski, J., Volpe, J., 2017. Cumulative effects of climate and landscape change drive spatial distribution of Rocky Mountain wolverine (Gulo gulo L.). Ecol. Evol. 7, 8903–8914. https://doi.org/10.1002/ece3.3337

Helbig, N., Bühler, Y., Eberhard, L., Deschamps-Berger, C., Gascoin, S., Dumont, M., Revuelto, J., Deems, J.S., Jonas, T., 2021. Fractional snow-covered area: scale-independent peak of winter parameterization. The Cryosphere 15, 615–632. https://doi.org/10.5194/tc-15-615-2021

Herman, J.D., Giuliani, M., 2018. Policy tree optimization for threshold-based water resources management over multiple timescales. Environ. Model. Softw. 99, 39–51. https://doi.org/10.1016/j.envsoft.2017.09.016

https://doi.org/10.5194/egusphere-2022-157
Preprint. Discussion started: 26 April 2022

Jennings, K.S., Winchell, T.S., Livneh, B., Molotch, N.P., 2018. Spatial variation of the rain–snow temperature threshold across the Northern Hemisphere. Nat. Commun. 9, 1148. https://doi.org/10.1038/s41467-018-03629-7

Jonas, T., Marty, C., Magnusson, J., 2009. Estimating the snow water equivalent from snow depth measurements in the Swiss Alps. J. Hydrol. 378, 161–167. https://doi.org/10.1016/j.jhydrol.2009.09.021

Kwadijk, J.C.J., Haasnoot, M., Mulder, J.P.M., Hoogvliet, M.M.C., Jeuken, A.B.M., van der Krogt, R.A.A., van Oostrom, N.G.C., Schelfhout, H.A., van Velzen, E.H., van Waveren, H., de Wit, M.J.M., 2010. Using adaptation tipping points to prepare for climate change and sea level rise: a case study in the Netherlands. WIREs Clim. Change 1, 729–740. https://doi.org/10.1002/wcc.64

Laliberte, A.S., Ripple, W.J., 2004. Range Contractions of North American Carnivores and Ungulates. BioScience 54, 123–138. https://doi.org/10.1641/0006-3568(2004)054[0123:RCONAC]2.0.CO;2

Liston, G.E., 2004. Representing Subgrid Snow Cover Heterogeneities in Regional and Global Models. J. Clim. 17, 1381–1397. https://doi.org/10.1175/1520-0442(2004)017<1381:RSSCHI>2.0.CO;2

Liston, G.E., Elder, K., 2006. A Distributed Snow-Evolution Modeling System (SnowModel). J. Hydrometeorol. 7, 1259–1276. https://doi.org/10.1175/JHM548.1

Liston, G.E., Perham, C.J., Shideler, R.T., Cheuvront, A.N., 2016. Modeling snowdrift habitat for polar bear dens. Ecol. Model. 320, 114–134. https://doi.org/10.1016/j.ecolmodel.2015.09.010

Livneh, B., Deems, J.S., Schneider, D., Barsugli, J.J., Molotch, N.P., 2014. Filling in the gaps: Inferring spatially distributed precipitation from gauge observations over complex terrain. Water Resour. Res. 50, 8589–8610. https://doi.org/10.1002/2014WR015442

Luce, C.H., Tarboton, D.G., Cooley, K.R., 1998. The influence of the spatial distribution of snow on basin-averaged snowmelt. Hydrol. Process. 12, 1671–1683. https://doi.org/10.1002/(SICI)1099-1085(199808/09)12:10/11<1671::AID-HYP688>3.0.CO;2-N

Lundquist, J.D., Dettinger, M.D., 2005. How snowpack heterogeneity affects diurnal streamflow timing. Water Resour. Res. 41. https://doi.org/10.1029/2004WR003649

Machguth, H., Paul, F., Hoelzle, M., Haeberli, W., 2006. Distributed glacier mass-balance modelling as an important component of modern multi-level glacier monitoring. Ann. Glaciol. 43, 335–343. https://doi.org/10.3189/172756406781812285

Magoun, A.J., Robards, M.D., Packila, M.L., Glass, T.W., 2017. Detecting snow at the den-site scale in wolverine denning habitat. Wildl. Soc. Bull. 41, 381–387. https://doi.org/10.1002/wsb.765

Maher, A.I., Treitz, P.M., Ferguson, M.A.D., 2012. Can Landsat data detect variations in snow cover within habitats of arctic ungulates? Wildl. Biol. 18, 75–87. https://doi.org/10.2981/11-055

Mahoney, P.J., Liston, G.E., LaPoint, S., Gurarie, E., Mangipane, B., Wells, A.G., Brinkman, T.J., Eitel, J.U.H., Hebblewhite, M., Nolin, A.W., Boelman, N., Prugh, L.R., 2018. Navigating snowscapes: scale-dependent responses of mountain sheep to snowpack properties. Ecol. Appl. 28, 1715–1729. https://doi.org/10.1002/eap.1773

Margulis, S.A., Cortés, G., Girotto, M., Durand, M., 2016. A Landsat-Era Sierra Nevada Snow Reanalysis (1985–2015). J. Hydrometeorol. 17, 1203–1221. https://doi.org/10.1175/JHM-D-15-0177.1

Margulis, S.A., Girotto, M., Cortés, G., Durand, M., 2015. A Particle Batch Smoother Approach to Snow Water Equivalent Estimation. J. Hydrometeorol. 16, 1752–1772. https://doi.org/10.1175/JHM-D-14-0177.1

Margulis, S.A., Liu, Y., Baldo, E., 2019. A Joint Landsat- and MODIS-Based Reanalysis Approach for Midlatitude Montane Seasonal Snow Characterization. Front. Earth Sci. 7. https://doi.org/10.3389/feart.2019.00272

McKelvey, K.S., Copeland, J.P., Schwartz, M.K., Littell, J.S., Aubry, K.B., Squires, J.R., Parks, S.A., Elsner, M.M., Mauger, G.S., 2011. Climate change predicted to shift wolverine distributions, connectivity, and dispersal corridors. Ecol. Appl. 21, 2882–2897. https://doi.org/10.1890/10-2206.1

Mote, P.W., Hamlet, A.F., Clark, M.P., Lettenmaier, D.P., 2005. DECLINING MOUNTAIN SNOWPACK IN WESTERN NORTH AMERICA*. Bull. Am. Meteorol. Soc. 86, 39–50. https://doi.org/10.1175/BAMS-86-1-39

Nolin, A.W., Daly, C., 2006. Mapping “at risk” snow in the Pacific Northwest. J. Hydrometeorol. 7, 1164–1171.

Pestana, S., Chickadel, C.C., Harpold, A., Kostadinov, T.S., Pai, H., Tyler, S., Webster, C., Lundquist, J.D., 2019. Bias Correction of Airborne Thermal Infrared Observations Over Forests Using Melting Snow. Water Resour. Res. 55, 11331–11343. https://doi.org/10.1029/2019WR025699

Pflug, J.M., Hughes, M., Lundquist, J.D., 2021. Downscaling snow deposition using historic snow depth patterns: Diagnosing limitations from snowfall biases, winter snow losses, and interannual snow pattern repeatability. Water Resour. Res. e2021WR029999. https://doi.org/10.1029/2021WR029999

https://doi.org/10.5194/egusphere-2022-157
Preprint. Discussion started: 26 April 2022

Pflug, J.M., Liston, G.E., Nijssen, B., Lundquist, J.D., 2019. Testing Model Representations of Snowpack Liquid Water Percolation Across Multiple Climates. Water Resour. Res. 55, 4820–4838. https://doi.org/10.1029/2018WR024632

Pflug, J.M., Lundquist, J.D., 2020. Inferring Distributed Snow Depth by Leveraging Snow Pattern Repeatability: Investigation Using 47 Lidar Observations in the Tuolumne Watershed, Sierra Nevada, California. Water Resour. Res. 56, e2020WR027243. https://doi.org/10.1029/2020WR027243

Sankey, T., Donald, J., McVay, J., Ashley, M., O'Donnell, F., Lopez, S.M., Springer, A., 2015. Multi-scale analysis of snow dynamics at the southern margin of the North American continental snow distribution. Remote Sens. Environ. 169, 307–319. https://doi.org/10.1016/j.rse.2015.08.028

Scott, J.D., Alexander, M.A., Murray, D.R., Swales, D., Eischeid, J., 2016. The Climate Change Web Portal: A System to Access and Display Climate and Earth System Model Output from the CMIP5 Archive. Bull. Am. Meteorol. Soc. 97, 523–530. https://doi.org/10.1175/BAMS-D-15-00035.1

Serreze, M.C., Clark, M.P., Armstrong, R.L., McGinnis, D.A., Pulwarty, R.S., 1999. Characteristics of the western United States snowpack from snowpack telemetry (SNO_{TEL}) data. Water Resour. Res. 35, 2145–2160. https://doi.org/10.1029/1999WR900090

Shih, J.-S., ReVelle, C., 1995. Water supply operations during drought: A discrete hedging rule. Eur. J. Oper. Res. 82, 163–175. https://doi.org/10.1016/0377-2217(93)E0237-R

Sivy, K.J., Nolin, A.W., Cosgrove, C.L., Prugh, L.R., 2018. Critical snow density threshold for Dall's sheep (Ovis dalli dalli). Can. J. Zool. 96, 1170–1177. https://doi.org/10.1139/cjz-2017-0259

USFWS, 2018. Species status assessment report for the North American Wolverine (Gulo gulo luscus). (No. Version 1.2.). U.S. Fish and Wildlife Service, Mountain-Prarie Region, Lakewood, CO.

Vögeli, C., Lehning, M., Wever, N., Bavay, M., 2016. Scaling Precipitation Input to Spatially Distributed Hydrological Models by Measured Snow Distribution. Front. Earth Sci. 4. https://doi.org/10.3389/feart.2016.00108

Wayand, N.E., Clark, M.P., Lundquist, J.D., 2017. Diagnosing snow accumulation errors in a rain-snow transitional environment with snow board observations. Hydrol. Process. 31, 349–363. https://doi.org/10.1002/hyp.11002

Wigmosta, M.S., Nijssen, B., Storck, P., Lettenmaier, D.P., 2002. The distributed hydrology soil vegetation model. Math. Models Small Watershed Hydrol. Appl. 7–42.

Xue, Y., Sellers, P.J., Kinter, J.L., Shukla, J., 1991. A Simplified Biosphere Model for Global Climate Studies. J. Clim. 4, 345–364. https://doi.org/10.1175/1520-0442(1991)004<0345:ASBMFG>2.0.CO;2

Yang, K., Musselman, K.N., Rittger, K., Margulis, S.A., Painter, T.H., Molotch, N.P., 2021. Combining ground-based and remotely sensed snow data in a linear regression model for real-time estimation of snow water equivalent. Adv. Water Resour. 104075. https://doi.org/10.1016/j.advwatres.2021.104075